500 nm System of RbCs: Assignments and Intensity Anomalies

Yonghoon Lee,*,†,⊥ Youngjee Yoon,‡,§ Sungyul Lee,|| and Bongsoo Kim*,‡

Advanced Photonics Research Institute, Gwangju Institute of Science and Technology, Gwangju 500-712, Korea, College of Environmental Science and Applied Chemistry, Kyunghee University, Kyungki-do 449-701, Korea, and Department of Chemistry, KAIST, Daejeon 305-701, Korea

Received: May 27, 2009; Revised Manuscript Received: September 2, 2009

We have investigated the RbCs 500 nm system by mass-resolved resonance enhanced two-photon ionization in a cold molecular beam. The 4 $^3\Pi_0$ v′ = 10−39, 4 $^3\Pi_1$ v′ = 14−28, and 6 $^1\Sigma^+$ v′ = 12−28 ← X $^1\Sigma^+$ v″ = 0 transitions have been observed and assigned for the first time. The 4 $^3\Pi_0$ v′ ← X $^1\Sigma^+$ v″ = 0 transitions abnormally show double maxima of the vibronic-band intensity distribution around v′ = 22 and 38. The intensities of the transitions to the lower vibrational levels (4 $^3\Pi_0$ v′ = 10−32) are explained well by the direct transitions from the X $^1\Sigma^+$ v″ = 0 level following the Franck−Condon principle. The transitions to the higher vibrational levels (4 $^3\Pi_0$ v′ ≥ 33) borrow intensities through the interaction with nearby 6 $^1\Sigma^+$ perturber levels.

1. Introduction

The ultracold molecules that have extremely low internal energies can be ideal samples for fundamental physics and chemistry.[1−7] Cold polar molecules attract particular interest because of their long-range anisotropic interactions[6] and prospect for a novel physical realization of a quantum computer.[8] DeMille proposed ultracold RbCs, produced by photoassociation of laser-cooled Rb and Cs atoms and the subsequent population transfer,[9] as one of the promising candidates for the quantum qubit generator.[8] As indicated by Ni et al., a suitable level in the excited electronic states should be employed for the stimulated Raman passage (STIRAP) to the ground X $^1\Sigma^+$ v = 0 level for efficient production of ultracold molecules.[1] Therefore, for the heteronuclear alkali dimers, information on the energy-level structures and perturbations of the excited states around equilibrium internuclear distances as well as the long-range data is quite desirable for the emerging molecular sciences with ultracold molecules.

For RbCs, several excited electronic states have been identified by resonance enhanced two-photon ionization (RE2PI) (4 $^1\Sigma^+$, 5 $^1\Sigma^+$, 3 $^1\Pi$, 2 $^3\Pi$, and 1 $^3\Delta$)[10−13] and laser-induced fluorescence (3 $^1\Sigma^+$, 4 $^1\Sigma^+$, 7 $^1\Sigma^+$, 2 $^1\Pi$, 4 $^1\Pi$, and 5 $^1\Pi$).[14,15] Detailed deperturbation analyses have been performed on the 2 $^1\Sigma^+$−1 $^3\Pi$ and 1 $^1\Pi$−2 $^3\Sigma^+$−1 $^3\Pi$ systems,[16,17] and the coupled 2 $^1\Pi$−2 $^3\Pi_1$−3 $^3\Sigma_1^+$ system[12] was identified recently. Very accurate theoretical calculations on the excited electronic states of RbCs have been reported since 2000.[18−21] The predicted electronic term values and equilibrium internuclear distances show discrepancies of less than 1−2% from the experimental values.[18]

In this work, we have investigated the complicated vibronic structures of RbCs near 500 nm by mass-resolved RE2PI spectroscopy in a cold molecular beam. The 4 $^3\Pi_0$ v′ = 10−39, 4 $^3\Pi_1$ v′ = 14−28, and 6 $^1\Sigma^+$ v′ = 12−28 ← X $^1\Sigma^+$ v″ = 0 transitions are newly identified. While the intensity distributions of the 4 $^3\Pi_0$ v′ ≤ 32 ← X $^1\Sigma^+$ v″ = 0 transitions are explained well by the Franck−Condon (FC) principle, the transitions to the higher levels (4 $^3\Pi_0$ v′ ≥ 33) show abnormally strong intensities. This is found to originate from the perturbation with the nearby bright 6 $^1\Sigma^+$ levels.

2. Experiment

Details of our experimental apparatus and techniques have been discussed previously.[22] Briefly, RbCs was produced by expanding Rb and Cs vapor with Kr or Ar gas through a high-temperature pulsed nozzle with a 800 μm diameter orifice. The alkali metal sample was heated to 350 °C. The pulsed jet was collimated by a 1.2 mm diameter skimmer. Two photons from a Nd:YAG pumped dye laser excited and ionized RbCs. The resulting ions of two isotopomers (^{85}Rb^{133}Cs and ^{87}Rb^{133}Cs) were separately and simultaneously detected by a linear time-of-flight (TOF) mass spectrometer ($m/\Delta m \approx 500$). Vibronic and rotational structures were revealed by 0.12 and 0.02 cm^{-1} laser resolutions ($\Delta\nu_{fwhm}$), respectively. Wavelength calibration of the dye laser was conducted using a wavemeter, Ne optogalvanic spectra, and I_2 LIF spectra[23] obtained simultaneously.

3. Results and Discussion

3.1. Assignments. Figure 1 shows the nonrelativistic ab initio potential energy curves (PECs) of the 5 $^1\Sigma^+$, 6 $^1\Sigma^+$, 4 $^1\Pi$, 5 $^3\Sigma^+$, and 4 $^3\Pi$ states.[18] The vertical dotted line represents the FC region excited from the X $^1\Sigma^+$ v = 0 level. Between 20000 and 21000 cm^{-1}, the inner walls of the 6 $^1\Sigma^+$ and 4 $^3\Pi$ PECs are located in the FC region. According to the selection rule of electric dipole transitions in Hund's case (c) ($\Delta\Omega = 0, \pm1$), two parallel ($\Delta\Omega = 0$, 6 $^1\Sigma^+$ and 4 $^3\Pi_0$ ← X $^1\Sigma^+$) transitions and one perpendicular ($\Delta\Omega = \pm1$, 4 $^3\Pi_1$ ← X $^1\Sigma^+$) transition are predicted to be observed in this energy region.[24]

Figure 2 shows the low-resolution RE2PI spectra of ^{85}RbCs and ^{87}RbCs isotopomers around 20000 cm^{-1} obtained by

* To whom correspondence should be addressed. E-mail: lyh@gist.ac.kr (Y.L.); bongsoo@kaist.ac.kr (B.K.). Fax: +82-62-970-3359 (Y.L.); +82-42-350-2810 (B.K.).
† Gwangju Institute of Science and Technology.
‡ KAIST.
§ Current Address: Memory Division, Samsung Electronics Co., LTD., Hwasung, Gyeonggi-do 445-701, Korea.
|| Kyunghee University.
⊥ Current Address: Department of Chemistry, Mokpo National University, Muan 534-729, Korea.

10.1021/jp904927u CCC: $40.75
Published on Web 09/30/2009

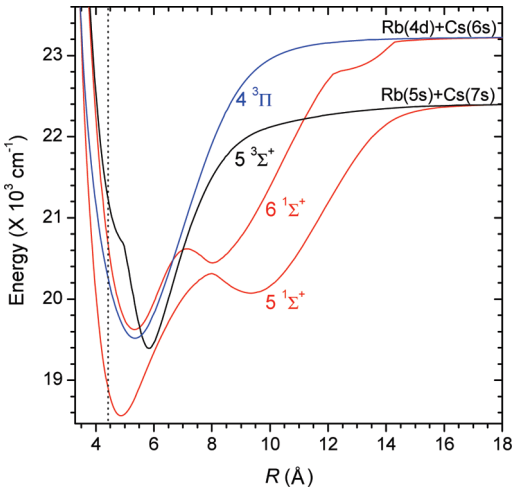

Figure 1. Nonrelativistic ab initio PECs of RbCs for the 5 $^1\Sigma^+$, 6 $^1\Sigma^+$, 5 $^3\Sigma^+$, and 4 $^3\Pi$ states from ref 18. The vertical dotted line represents the FC region (R_e of the $X\ ^1\Sigma^+$ state, 4.379 Å from ref 18). The origin of the ordinate axis is set to the potential minimum of the $X\ ^1\Sigma^+$ state.

coexpanding Kr carrier gas at 760 Torr. In the energy region below 20410 cm^{-1} (region I), four vibrational progressions, denoted as α, β, γ, and δ in Figure 2, are identified. Above 20410 cm^{-1} (region II), the spectra show very complex and rich vibronic structures. Here, we focus on the vibronic structures and intensity distributions in region I. The vibronic-band intensity distribution of the β progression shows double maxima around 19950 and 20375 cm^{-1}. This is very abnormal because the Franck−Condon distribution of vibronic-band intensities from the $X\ ^1\Sigma^+$ $v'' = 0$ level can never have more than one maximum aside from very unusual R-dependence of the transition moment function or strong perturbation effects. Despite the intensity anomalies and significant red shifts of the vibronic bands, the vibrational spacing of the β progression shows a smooth connection at around 20225 cm^{-1}. The plot of the vibrational spacing of the β progression can be found in the Supporting Information. The vibronic-band intensity anomalies in the β progression will be discussed in section 3.2.

The upper electronic states of α, β, γ, and δ progressions are assigned as follows. The α progression is easily assigned to the 5 $^1\Sigma^+$ $v' = 29-35 \leftarrow X\ ^1\Sigma^+$ $v'' = 0$ transitions by comparing the observed vibronic-band positions with those reported by Yoon et al.[11] Candidates for the upper electronic states of the β, γ, and δ progressions are the 6 $^1\Sigma^+$, 4 $^3\Pi_0$, and 4 $^3\Pi_1$ states, as predicted by theoretical calculations.[18−20] The β and γ bands progress parallel to each other with an almost constant spacing between the nearby bands. This indicates that their upper electronic states are the $\Omega = 0$ ($\Lambda = 1$, $\Sigma = -1$) and 1 ($\Lambda = 1$, $\Sigma = 0$) substates of the 4 $^3\Pi$ state. In this case, the shapes of both PECs in Hund's case (c) would be very similar and split by the magnitude of the 4 $^3\Pi$ diagonal spin−orbit (SO) interaction constant.[24] The upper-state Ω (Ω′) values of the β and γ bands are assigned below by their rotational structures. Then, the upper electronic state of the δ progression is assigned logically to the 6 $^1\Sigma^+$ state.

Absolute vibrational quantum numbers can be determined from the isotope shifts, $\Delta T_{v'} = T_{v'}(^{85}\text{RbCs}) - T_{v'}(^{87}\text{RbCs})$.[12,25] The vibrational term values, $T_{v'}$, of isotopomers were fitted simultaneously by the following mass-reduced relation:

$$T_{v'} = T_e + \omega_e\rho(v' + 1/2) - \omega_e x_e[\rho(v' + 1/2)]^2 \quad (1)$$

T_e, ω_e, and $\omega_e x_e$ are the electronic term value, harmonic vibrational frequency, and anharmonic vibrational constant, respectively. The constant ρ (=1 for ^{85}RbCs and 0.992963624 for ^{87}RbCs)[26] is $(\mu/\mu_{iso})^{1/2}$, where μ and μ_{iso} are the reduced masses of ^{85}RbCs and ^{87}RbCs, respectively. The vibronic bands in the ranges of $v' = 10-32$, 14−28, and 12−23 were fitted for β, γ, and δ progressions, respectively. The expected $\Delta T_{v'}$ values were calculated from the fitted parameters using the following equation:

$$\Delta T_{v'} = \omega_e(v' + 1/2) - \omega_e x_e(v' + 1/2)^2 - [\omega_e\rho(v' + 1/2) - \omega_e x_e\rho^2(v' + 1/2)^2] \quad (2)$$

Figure 3 compares the observed isotope shifts of the β, γ, and δ bands and the calculated values. For the calculations, v''s of the lowest-lying β, γ, and δ bands were assumed to be 9, 10, and 11 (for β), 13, 14, and 15 (for γ), and 11, 12, and 13 (for δ). The assigned v''s of the lowest-lying β, γ, and δ bands are designated for each progression in Figure 2. On this basis, we assign minimum $v' = 10$, 14, and 12 to the β, γ, and δ bands, respectively.

The Ω′ values of β and γ bands are revealed by their rotational structures. Parallel and perpendicular electric dipole transitions can be distinguished by rotational branches of an observed vibronic band.[24] Parallel bands ($\Delta\Lambda = 0$ in Hund's case (a) or $\Delta\Omega = 0$ in Hund's case (c)) consist of P ($\Delta J = -1$) and R ($\Delta J = +1$) branches of similar intensity. Perpendicular bands ($\Delta\Lambda = \pm 1$ in Hund's case (a) or $\Delta\Omega = \pm 1$ in Hund's case (c)) have a strong Q ($\Delta J = 0$) branch of approximately twice the intensity of the P and R branches. Figure 4 compares the rotationally resolved spectra of the β ($v' = 17 \leftarrow v'' = 0$), γ ($v' = 21 \leftarrow v'' = 0$), and δ ($v' = 23 \leftarrow v'' = 0$) bands with the simulations assuming $\Omega' = 0$ and 1. The experimental spectra were analyzed by line position fits using the following equation:

$$\nu = \nu_0 + B_{v'}J'(J' + 1) - D_{v'}[J'(J' + 1)]^2 - \{B_{v''}J''(J'' + 1) - D_{v''}[J''(J'' + 1)]^2\} \quad (3)$$

ν, ν_0, $B_{v'}$, $B_{v''}$, $D_{v'}$, $D_{v''}$, J', and J'' are the observed rotational line position, band origin, upper- and lower-state rotational constants, upper- and lower-state centrifugal distortion constants, and upper- and lower-state rotational quantum numbers, respectively. $B_{v''}$ (=0.016592237 cm^{-1}) and $D_{v''}$ (=7.3075 × 10^{-9} cm^{-1}) were fixed at the values reported by Fellows et al.[27] In our experiment, the rovibronic transitions are limited to low J' levels less than 26. Thus, the $D_{v'}$ values could not be determined accurately and were not included in the final fit. The observed rotational line positions, their assignments of J' and J'' numbers, and the fitted band origins and $B_{v'}$ values can be found in the Supporting Information. As shown in Figure 4, the β ($v' = 17 \leftarrow v'' = 0$) bands show both P and R branches ($\Omega' = 0$) and the γ ($v' = 21 \leftarrow v'' = 0$) band is closer to the simulation with $\Omega' = 1$ than that with $\Omega' = 0$. Consequently, the upper electronic states of β and γ progressions are assigned to the 4 $^3\Pi_0$ and 4 $^3\Pi_1$ states, respectively. For the δ ($v' = 23 \leftarrow v'' = 0$) band, the simulation indicates that the Ω′ value is 0, confirming the assignment of the upper electronic state to the 6 $^1\Sigma^+$ state.

In Table 1, the experimentally determined and theoretically predicted molecular constants[18,20] are listed. Comparing the experimental and theoretical T_e and ω_e values, the upper

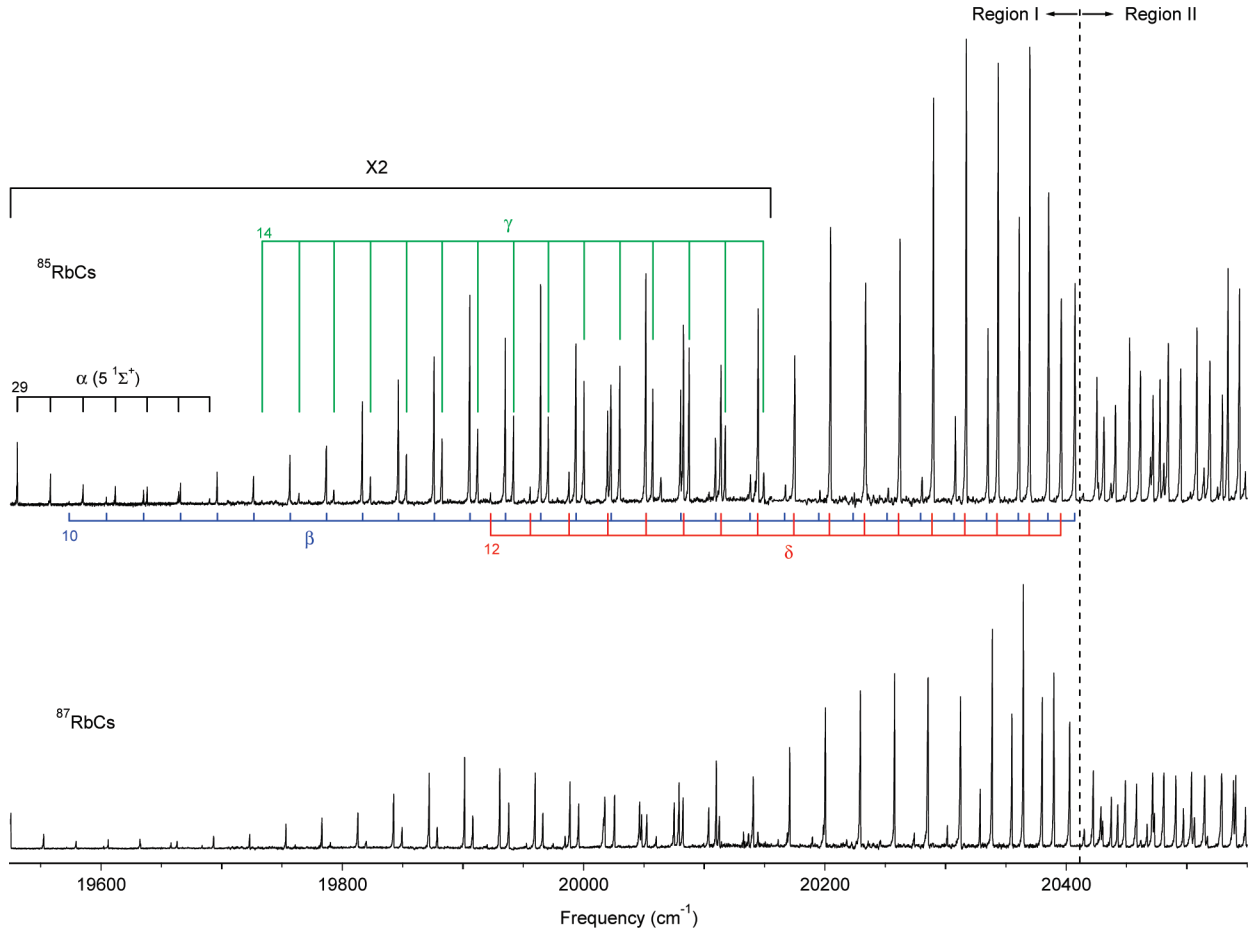

Figure 2. Low-resolution RE2PI spectra of (top) ^{85}RbCs and (bottom) ^{87}RbCs between 19525 and 20550 cm^{-1} obtained by expanding Kr carrier gas at 760 Torr. α, β, γ, and δ progressions and their vibrational quantum numbers are indicated.

electronic states of the β, γ, and δ bands are assigned to 4 $^3\Pi_0$, 4 $^3\Pi_1$, and 6 $^1\Sigma^+$, respectively. This is consistent with the assignment from the rotational structures. The lists of $T_{v'}$ values of the β, γ, and δ bands are given in the Supporting Information.

The diagonal matrix element of the SO coupling operator observed as the splitting of fine-structure levels is expressed as $\langle \Lambda, \Sigma, \Omega, v|H^{SO}|\Lambda, \Sigma, \Omega, v\rangle = A_{\Lambda,v}\Lambda\Sigma$.[24] For the $^3\Pi$ state, this indicates that the vibrational levels of the different Ω (=0, 1, and 2) substates are equally separated by the SO coupling constant, A_v. From this analysis, the 4 $^3\Pi$ state is found to be split by 70 cm^{-1} (T_e = 19262 cm^{-1} for 4 $^3\Pi_0$ and T_e = 19332 cm^{-1} for 4 $^3\Pi_1$). This becomes an estimation of the SO coupling constant of the 4 $^3\Pi$ state.

3.2. Intensity Anomalies. Figure 5 shows (a) the observed vibronic-band intensity distributions of the β and δ progressions and (b) the FC factors of the 4 $^3\Pi_0$ $v_\Pi \leftarrow X\ ^1\Sigma^+$ $v_X = 0$ ($|\langle v_\Pi|v_X\rangle|^2$) and 6 $^1\Sigma^+$ $v_\Sigma \leftarrow X\ ^1\Sigma^+$ $v_X = 0$ ($|\langle v_\Sigma|v_X\Sigma\rangle|^2$) transitions. The FC factors were calculated by the LEVEL 7.7 program[28] using the empirical PEC of the 4 $^3\Pi_0$ state and the modified PEC of the 6 $^1\Sigma^+$ state from the ab initio PEC.[18] The empirical PEC of the 4 $^3\Pi_0$ state was constructed by the Rydberg−Klein−Rees (RKR) method[29] using the experimentally determined vibrational and rotational constants. The rotational constants were determined by analyses of rotationally resolved spectra of the β (v' = 16−25 ← v'' = 0) bands. See the Supporting Information for the plot of the determined $B_{v'}$ values of the β bands as a function of v'. For the 6 $^1\Sigma^+$ state, the energy of the *ab initio* PEC was scaled by a factor of 0.9365 with respect to T_e and then T_e was set to the experimental value. As mentioned above, the observed vibronic-band intensity distribution of the β progression shows double maxima around v' = 22 and 38. The intensity distribution of the lower-lying β bands ($v' \leq 32$) is explained well by the FC principle (compare the observed and calculated values in Figures 5a and 6b, respectively). However, the dramatic increase in the intensities of the higher-lying β bands ($v' \geq 33$) cannot be rationalized by the direct vertical transitions from the $X\ ^1\Sigma^+$ $v'' = 0$ level. In this energy region, we can define the 6 $^1\Sigma^+$ state as the "bright" state and the 4 $^3\Pi_0$ state as the "dark" state. The former can be directly excited from the $X\ ^1\Sigma^+$ $v_X = 0$ level. On the other hand, direct transitions to the vibrational levels of the latter from the $X\ ^1\Sigma^+$ $v_X = 0$ level are almost impossible due to very small FC factors. No bright states other than the 6 $^1\Sigma^+$ state are predicted by *ab initio* calculations in the FC region around 20400 cm^{-1}. When a dark state interacts with a bright state, the borrowed transition moment can be estimated as follows:[24]

$$\langle \text{Dark}, v_{\text{Dark}}|\mu|X\ ^1\Sigma^+, v_X = 0\rangle = \sum_{v_{\text{Bright}}} \langle \text{Bright}|\mu|X\ ^1\Sigma^+\rangle\langle v_{\text{Bright}}|v_X = 0\rangle\langle \text{Dark}|H^{SO}|\text{Bright}\rangle \frac{\langle v_{\text{Dark}}|v_{\text{Bright}}\rangle}{E(v_{\text{Dark}}) - E(v_{\text{Bright}})} \quad (4)$$

The first two terms in the above equation are the electric dipole transition moment and the FC factor between bright and ground states. The third term is the interaction matrix element between dark and bright states. In this case, we assume that the interaction is SO coupling, H^{SO}, between the 4 $^3\Pi_0$ and 6 $^1\Sigma^+$ states. The

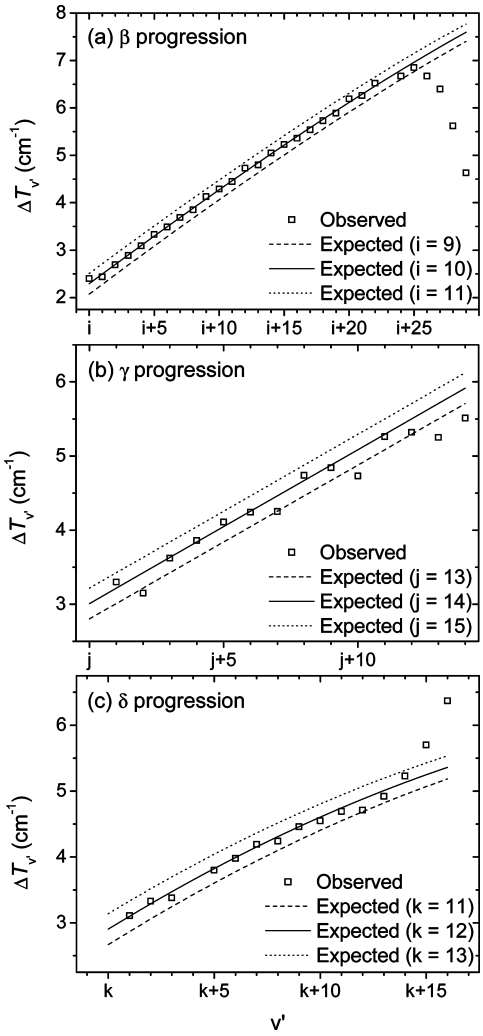

Figure 3. Observed isotope shifts of (a) β, (b) γ, and (c) δ progressions between ^{85}RbCs and ^{87}RbCs and the expected values assuming v′′s of the lowest-lying β, γ, and δ bands to be 9, 10, and 11 (for β), 13, 14, and 15 (for γ), and 11, 12, and 13 (for δ).

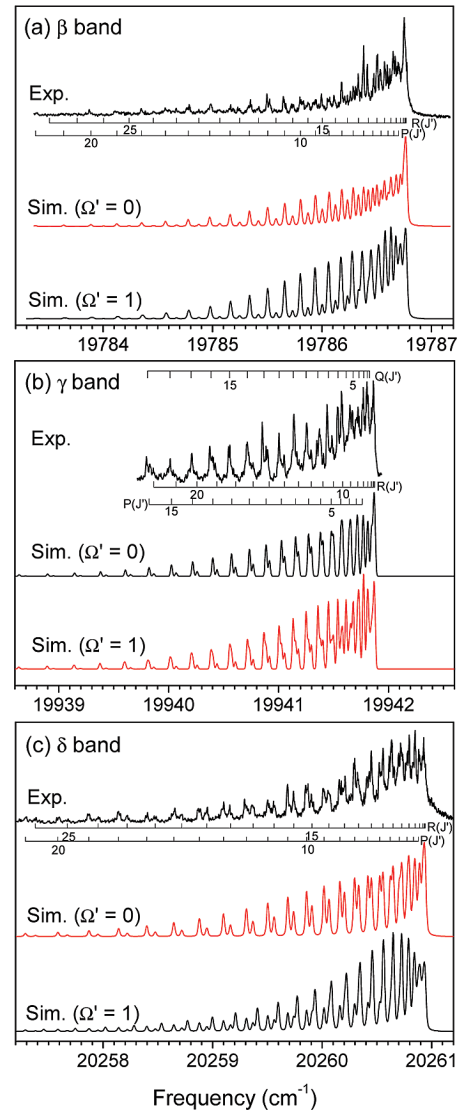

Figure 4. High-resolution RE2PI spectra of the (a) β ($v' = 17 \leftarrow v'' = 0$), (b) γ ($v' = 21 \leftarrow v'' = 0$), and (c) δ ($v' = 23 \leftarrow v'' = 0$) bands, and their simulations as parallel ($\Omega' = 0 \leftarrow \Omega'' = 0$) and perpendicular ($\Omega' = 1 \leftarrow \Omega'' = 0$) bands. For the simulations, rotational temperatures were set to 2.3, 2.4, and 2.6 K for the β, γ, and δ bands, respectively, and the stick spectra were convoluted by a Voit profile ($\Delta\nu_{Gauss} = 0.02$ cm^{-1} and $\Delta\nu_{Lorent} = 0.01$ cm^{-1}). Between the simulations assuming $\Omega' = 0$ and 1, the better fit is shown in red.

last term is the vibrational overlap between dark and bright states divided by their energy level difference. The intensity borrowing mechanism of the dark state is, thus, described by the last two terms.

The 4 $^3\Pi_0$−6 $^1\Sigma^+$ vibrational overlap, $\langle v_\Pi | v_\Sigma \rangle$, values were calculated by the LEVEL 7.7 program[28] using the same PECs employed for the calculation of FC factors shown in Figure 5b. From this calculation, we can gain an insight into the intensity borrowing mechanisms of the dark 4 $^3\Pi_0$ levels. Figure 6 shows the maps of (a) $\langle v_\Pi | v_\Sigma \rangle$ and (b) $\langle v_\Pi | v_\Sigma \rangle / |\Delta E|$, and the bar graphs of (c) $\langle v_\Pi = 37 | v_\Sigma \rangle$ and (d) $\langle v_\Pi = 37 | v_\Sigma \rangle / |\Delta E|$. ΔE is the energy difference between v_Σ and v_Π levels, $E(v_\Sigma) - E(v_\Pi)$. The two-dimensional maps of $\langle v_\Pi | v_\Sigma \rangle$ and $\langle v_\Pi | v_\Sigma \rangle / |\Delta E|$ are plotted for the v_Π levels between 20000 and 20700 cm^{-1} and the v_Σ levels between 20200 and 21000 cm^{-1}. In Figure 6a and b, white and red dotted lines indicate the regions of $\Delta E \approx 200$ and 0 cm^{-1}, respectively. The energy at the top of the barrier between the inner and outer wells of the 6 $^1\Sigma^+$ double-minimum PEC is also indicated by the arrows in Figure 6a and b. The map shown in Figure 6a indicates that the remote v_Σ levels ($\Delta E \approx 200$ cm^{-1}) provide the dark v_Π levels with particularly large $\langle v_\Pi | v_\Sigma \rangle$ values. However, when ΔE is taken into account, the nearby v_Σ levels ($\Delta E \approx 0$ cm^{-1}) are found to be more important to the intensity borrowing of the dark v_Π levels. This energy-level proximity effect on the intensity borrowing of the 4 $^3\Pi_0$ dark levels is shown for the $v_\Pi = 37$ level in Figure 6c and d. The horizontal dotted lines in Figure 6c and d indicate the energy of the $v_\Pi = 37$ level at 20385 cm^{-1}. Due to the energy-level proximity effect, the contribution of the nearby v_Σ perturbers to the borrowed transition moment of the $v_\Pi = 37$ level becomes ~20 times

TABLE 1: Experimental and Theoretical Molecular Constants

		T_e (cm^{-1})	ω_e (cm^{-1})	$\omega_e x_e$ (cm^{-1})	R_e (Å)
β [4 $^3\Pi_0$]		19262.10(82)	33.238(17)	0.134(13)	
γ [4 $^3\Pi_1$]		19332.02(82)	29.497(37)		
δ [6 $^1\Sigma^+$]		19504.46(91)	37.92(11)	0.1971(31)	
4 $^3\Pi$	theory 1[a]	19517	33		5.350
	theory 2[b]	19384	34		5.420
6 $^1\Sigma^+$	theory 1[a]	19624	35		5.332
	theory 2[b]	19477	36		5.436

[a] Reference 18. [b] Reference 20.

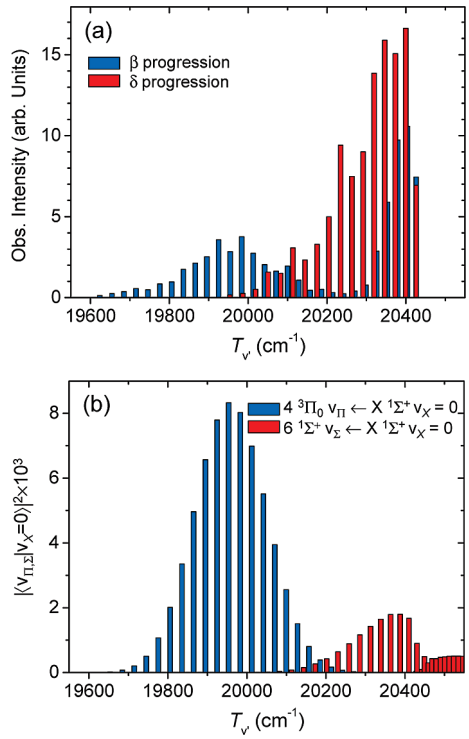

Figure 5. (a) The observed vibronic-band intensity distributions of β and δ progressions. (b) The $|\langle v_\Pi|v_X\rangle|^2$ and $|\langle v_\Sigma|v_X\rangle|^2$ values calculated using the RKR PECs for the 4 $^3\Pi_0$ (see the Supporting Information) and X $^1\Sigma^+$ states (ref 27) and the modified PEC from the ab initio one for 6 $^1\Sigma^+$ (ref 18).

larger than that of the remote v_Σ perturbers. Figure 7 shows the vibrational wave functions of the $v_\Pi = 37$ level at 20385 cm^{-1} and the two v_Σ levels at 20381 (nearby) and 20589 (remote) cm^{-1}. Between the v_Π and nearby v_Σ levels, the $\langle v_\Pi|v_\Sigma\rangle$ value (0.042) is mostly contributed by the 4 $^3\Pi_0$−6 $^1\Sigma^+$ PEC crossing region. At the stationary phase point, the momenta are matched and the overlap integral accumulates. In other regions, $\langle v_\Pi|v_\Sigma\rangle$ is canceled out by the out-of-phase oscillations of the wave functions. Between the v_Π and remote v_Σ level, the $\langle v_\Pi|v_\Sigma\rangle$ value (0.088) is larger than that between the nearby v_Π and v_Σ levels. As shown in Figure 6a (see the region indicated by the white dotted line), the v_Π levels have the largest $\langle v_\Pi|v_\Sigma\rangle$ with the remote v_Σ levels. This is due to the in-phase oscillations of both vibrational wave functions. However, this large $\langle v_\Pi|v_\Sigma\rangle$ is not effective because of large energy differences.

Consequently, we have found that the abnormally strong intensities of the β ($v' = 33-39 \leftarrow v'' = 0$) bands observed in the RE2PI spectra (see Figure 2) originate from the perturbations between the 4 $^3\Pi_0$ and 6 $^1\Sigma^+$ states, and the nearby 6 $^1\Sigma^+$ perturber levels dominantly contribute to the intensity borrowing through the energy-level proximity effect. Figure 8 shows the differences between the fitted and observed $T_{v'}$s for the β progression, $T_{v'}^{fit} - T_{v'}^{obs}$. The 4 $^3\Pi_0$ $v' = 33-39$ levels are significantly red-shifted. This also indicates the existence of the nearby blue-side perturbers. Therefore, the whole vibronic-band intensity distribution of the 4 $^3\Pi_0$ $v' = 10-39 \leftarrow$ X $^1\Sigma^+$ $v'' = 0$ transitions comes from two different intensity borrowing mechanisms: (i) from the 6 $^1\Sigma^+$ remote perturber ($\Delta E \sim 200$ cm^{-1}) to the lower-lying 4 $^3\Pi_0$ v' levels and (ii) from the 6 $^1\Sigma^+$ nearby perturber ($\Delta E \sim 0$ cm^{-1}) to the higher-lying ones. When multiple perturbers make comparable contributions to intensity borrowing of a dark state, the interference effects on the borrowed transition moments should be considered. Rotas et al. reported the representative example of the multiple-perturber

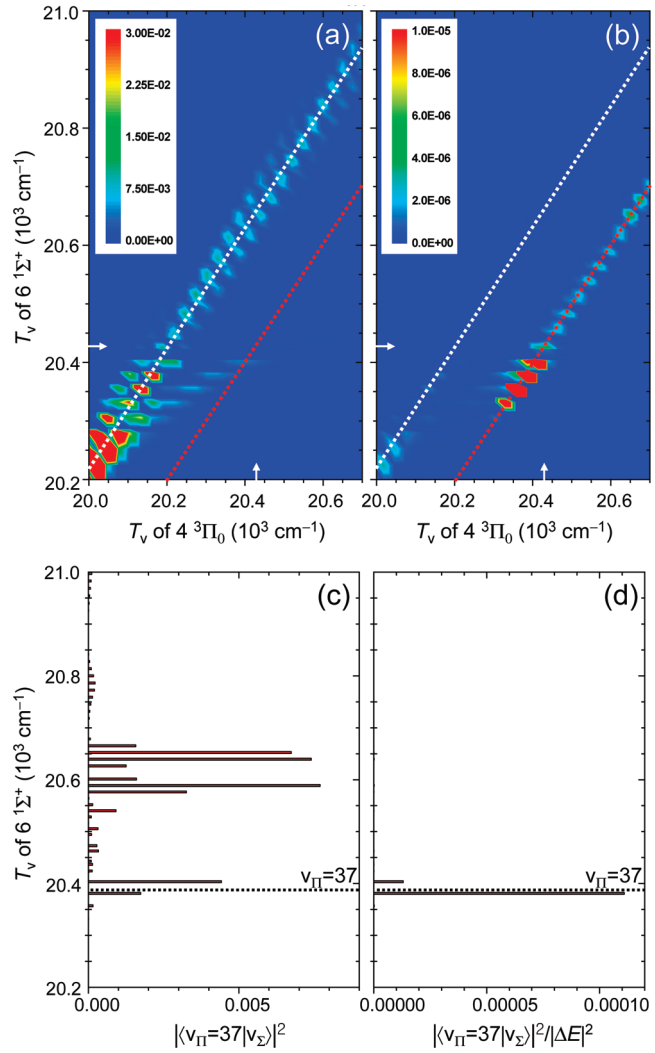

Figure 6. Maps of (a) $|\langle v_\Pi|v_\Sigma\rangle|^2$ and (b) $|\langle v_\Pi|v_\Sigma\rangle|^2/|\Delta E|^2$ and the bar graphs of (c) $|\langle v_\Pi = 37|v_\Sigma\rangle|^2$ and (d) $|\langle v_\Pi = 37|v_\Sigma\rangle|^2/|\Delta E|^2$. In the maps of $|\langle v_\Pi|v_\Sigma\rangle|^2$ and $|\langle v_\Pi|v_\Sigma\rangle|^2/|\Delta E|^2$, the regions of $\Delta E = 200$ and 0 cm^{-1} are indicated by white and red dotted lines, respectively, and the energy at the top of the barrier between the inner and outer wells of the 6 $^1\Sigma^+$ PEC is indicated by arrows. In the bar graphs of $|\langle v_\Pi = 37|v_\Sigma\rangle|^2$ and $|\langle v_\Pi = 37|v_\Sigma\rangle|^2/|\Delta E|^2$, the energy of the $v_\Pi = 37$ level (20385 cm^{-1}) is indicated by the horizontal dotted line.

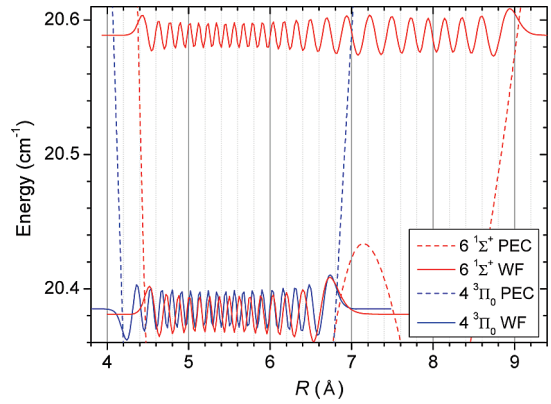

Figure 7. Vibrational wave functions of the $v_\Pi = 37$ level at 20385 cm^{-1} (blue solid line) and the two v_Σ levels at 20381 and 20589 cm^{-1} (red solid lines), and PECs of the 4 $^3\Pi_0$ (blue dotted line) and 6 $^1\Sigma^+$ (red dotted line) states.

contributions on the nominally spin-forbidden transitions.[30] Here, it is worth considering whether the two different intensity

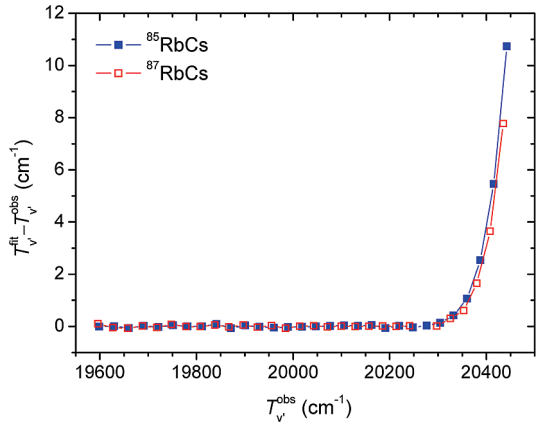

Figure 8. Differences between the fitted and observed $T_{v'}$'s for the β progression, $T_{v'}^{fit} - T_{v'}^{obs}$.

borrowing mechanisms of the 4 $^3\Pi_0$ v′ ← X $^1\Sigma^+$ v″ = 0 transitions can interfere or not. As shown in Figure 2, the two vibronic-band intensity distributions of 4 $^3\Pi_0$ v′← X $^1\Sigma^+$ v″ = 0 around v′ = 22 and 38 are almost completely separated. This indicates the two different mechanisms dominate the 4 $^3\Pi_0$ v′← X $^1\Sigma^+$ v″ = 0 transitions in the different energy regions (divided at 20225 cm^{-1}). Under these circumstances, they can hardly interfere with each other.

The 4 $^3\Pi_0$ dark levels above the barrier energy of the 6 $^1\Sigma^+$ PEC can borrow the transition moments from the nearby 6 $^1\Sigma^+$ levels (see Figure 6b). As shown in Figure 2, the vibronic structures in region II become very dense and complicated. The dense vibronic structure is probably due to abrupt expansion of the 6 $^1\Sigma^+$ potential well above the barrier energy. The transitions to the higher 4 $^3\Pi_0$ dark levels, however, may also contribute to the complicated vibronic spectra above 20410 cm^{-1}.

4. Conclusion

We have assigned the 4 $^3\Pi_0$ v′ = 10−39, 4 $^3\Pi_1$ v′ = 14−28, and 6 $^1\Sigma^+$ v′ = 12−28 ← *X* $^1\Sigma^+$ v″ = 0 transitions of RbCs near 500 nm for the first time. For the 4 $^3\Pi_0$ v′ = 10−39 ← *X* $^1\Sigma^+$ v″ = 0 transitions, abnormal double maxima of the vibronic-band intensity distribution were observed. The FC principle explains the intensity distribution of the 4 $^3\Pi_0$ v′ = 10−32 ← *X* $^1\Sigma^+$ v″ = 0 transitions well. However, the vibrational levels around the higher-lying maximum (4 $^3\Pi_0$ v′ = 33−39) cannot be directly excited from the *X* $^1\Sigma^+$ v″ = 0 level because of negligible FC factors. We suggest the intensity borrowing mechanism of the transitions to the dark 4 $^3\Pi_0$ levels. The nearby bright 6 $^1\Sigma^+$ levels have been found to shed light on the 4 $^3\Pi_0$ levels.

Acknowledgment. This work was supported by National Research Foundation of Korea Grant funded by Korean Government (2009-0071746), SRC through the Center for Intelligent Nano-Bio Materials (R11-2005-008-03001-1-0), and Asian Laser Center Program through a grant provided by the Gwangju Institute of Science and Technology in 2009. S.L. acknowledges financial support by Kyunghee University 2008.

Supporting Information Available: Data of the RbCs 500 nm system by RE2PI spectroscopy: (i) a plot of the vibrational spacing, $\Delta G_{v'}$, of β bands as a function of v′; (ii) observed rotational line positions, their assignments of J' and J'' numbers, and the fitted band origins and $B_{v'}$ values of the β (v′ = 17 ← v″ = 0), γ (v′ = 21 ← v″ = 0), and δ (v′ = 23 ← v″ = 0) bands; (iii) lists of $T_{v'}$ values of β, γ, and δ progressions; and (iv) a plot of $B_{v'}$ values of β bands as a function of v′. This material is available free of charge via the Internet at http://pubs.acs.org.

References and Notes

(1) Ni, K.-K.; Ospelkaus, S.; de Miranda, M. H. G.; Pe'er, A.; Neyenhuis, B.; Zirbel, J. J.; Kotochigova, S.; Julienne, P. S.; Jin, D. S.; Ye, J. *Science* **2008**, *322*, 231.
(2) Ospelkaus, S.; Pe'er, A.; Ni, K.-K.; Zirbel, J. J.; Neyenhuis, B.; Kotochigova, S.; Julienne, P. S.; Ye, J.; Jin, D. S. *Nat. Phys.* **2008**, *4*, 622.
(3) Danzl, J. G.; Haller, E.; Gustavsson, M.; Mark, M. J.; Hart, R.; Bouloufa, N.; Dulieu, O.; Ritsch, H.; Nägerl, H.-C. *Science* **2008**, *321*, 1062.
(4) Viteau, M.; Chotia, A.; Allegrini, M.; Bouloufa, N.; Dulieu, O.; Comparat, D.; Pillet, P. *Science* **2008**, *321*, 232.
(5) Bauer, D. M.; Lettner, M.; Vo, C.; Rempe, G.; Dürr, S. *Nat. Phys.* **2009**, *5*, 339.
(6) Büchler, H. P.; Demler, E.; Lukin, M.; Micheli, A.; Prokof'ev, N.; Pupillo, G.; Zoller, P. *Phys. Rev. Lett.* **2007**, *98*, 060404.
(7) Krems, R. V. *Phys. Chem. Chem. Phys.* **2008**, *10*, 4079.
(8) DeMille, D. *Phys. Rev. Lett.* **2002**, *88*, 067901.
(9) Sage, J. M.; Sainis, S.; Bergeman, T.; DeMille, D. *Phys. Rev. Lett.* **2005**, *94*, 203001.
(10) Kim, B.; Yoshihara, K. *J. Chem. Phys.* **1994**, *100*, 1849.
(11) Yoon, Y.; Lee, Y.; Kim, T.; Ahn, J. S.; Jung, Y.; Kim, B.; Lee, S. *J. Chem. Phys.* **2001**, *114*, 8926.
(12) Lee, Y.; Yoon, Y.; Lee, S.; Kim, J.-T.; Kim, B. *J. Phys. Chem. A* **2008**, *112*, 7214.
(13) Kim, B.; Yoshihara, K. *Chem. Phys. Lett.* **1993**, *212*, 271.
(14) Gustavsson, T.; Amiot, C.; Vergès, J. *Mol. Phys.* **1988**, *64*, 293.
(15) Nogueira, A.; Fellows, C. E.; Bergeman, T. *J. Chem. Phys.* **2008**, *129*, 136101.
(16) Bergeman, T.; Fellows, C. E.; Gutterres, R. F.; Amiot, C. *Phys. Rev. A* **2003**, *67*, 050501(R).
(17) Bergeman, T.; Kerman, A. J.; Sage, J.; Sainis, S.; DeMille, D. *Eur. Phys. J. D* **2004**, *31*, 179.
(18) Allouche, A. R.; Korek, M.; Fakherddin, K.; Chaalan, A.; Dagher, M.; Taher, F.; Aubert-Frécon, M. *J. Phys. B: At. Mol. Opt. Phys.* **2000**, *33*, 2307.
(19) Fahs, H.; Allouche, A. R.; Korek, M.; Aubert-Frécon, M. *J. Phys. B: At. Mol. Opt. Phys.* **2002**, *35*, 1501.
(20) Lim, I. S.; Lee, W. C.; Lee, Y. S.; Jeung, G.-H *J. Chem. Phys.* **2006**, *124*, 234307.
(21) Kotochigova, S.; Tiesinga, E. *J. Chem. Phys.* **2005**, *123*, 174304.
(22) Lee, Y.; Yoon, Y.; Baek, S. J.; Joo, D.-L.; Ryu, J.-S.; Kim, B. *J. Chem. Phys.* **2000**, *113*, 2116.
(23) Gerstenkorn, S.; Luc, P. *Atlas du Spectre d'Absorption de la Molécule d'Iode Entre 14800−20000 cm^{-1}*; CNRS: Paris, 1978.
(24) Lefebvre-Brion, H.; Field, R. W. *The Spectra and Dynamics of Diatomic Molecules*; Elsevier: New York, 2004.
(25) Lee, Y.; Lee, S.; Kim, B. *J. Phys. Chem. A* **2007**, *111*, 11750.
(26) Mills, I.; Cvitaš, T.; Homann, K.; Kallay, N.; Kuchitsu, K. *Quantities, Units and Symbols in Physical Chemistry*; Blackwell: Oxford, U.K., 1993.
(27) Fellows, C. E.; Gutterres, R. F.; Campos, A. P. C.; Vergès, J; Amiot, C. *J. Mol. Spectrosc.* **1999**, *197*, 19.
(28) Le Roy, R. J. *LEVEL 7.7. A Computer Program for Solving the Radial Schrödinger Equation for Bound and Quasibound Levels*; University of Waterloo Chemical Physics Research Report CP-661; University of Waterloo: Ontario, Canada, 2005.
(29) Le Roy, R. J. *RKR1 2.0. A Computer Program for Implementing the First-Order RKR Method for Determining Diatomic Molecule Potential Energy Curves*; University of Waterloo Chemical Physics Research Report CP-657R; University of Waterloo: Ontario, Canada, 2004.
(30) Rostas, F.; Eidelsberg, M.; Jolly, A.; Lemaire, J. L.; Le Floch, A.; Rostas, J. *J. Chem. Phys.* **2000**, *112*, 4591.

JP904927U